JOURNAL OF GEOPHYSICAL RESEARCH, VOL. 108, NO. D19, 4604, doi:10.1029/2002JD003054, 2003

Nonmethane hydrocarbons and ozone in three rural southeast United States national parks: A model sensitivity analysis and comparison to measurements

Daiwen Kang[1] and Viney P. Aneja
Department of Marine, Earth, and Atmospheric Sciences, North Carolina State University, Raleigh, North Carolina, USA

Rohit Mathur
Carolina Environmental Program, University of North Carolina, Chapel Hill, North Carolina, USA

John D. Ray
Air Resources Division, National Park Service, Denver, Colorado, USA

Received 18 October 2002; revised 28 April 2003; accepted 24 July 2003; published 8 October 2003.

[1] A detailed modeling analysis is conducted focusing on nonmethane hydrocarbons and ozone in three southeast United States national parks for a 15-day time period (14–29 July 1995) characterized by high O_3 surface concentrations. The three national parks are Smoky Mountains National Park (GRSM), Mammoth Cave National Park (MACA), and Shenandoah National Park (SHEN), Big Meadows. A base emission scenario and eight variant predictions are analyzed, and predictions are compared with data observed at the three locations for the same time period. Model-predicted concentrations are higher than observed values for O_3 (with a cutoff of 40 ppbv) by 3.0% at GRSM, 19.1% at MACA, and 9.0% at SHEN (mean normalized bias error). They are very similar to observations for overall mean ozone concentrations at GRSM and SHEN. They generally agree (the same order of magnitude) with observed values for lumped paraffin compounds but are an order of magnitude lower for other species (isoprene, ethene, surrogate olefin, surrogate toluene, and surrogate xylene). Model sensitivity analyses here indicate that each location differs in terms of volatile organic compound (VOC) capacity to produce O_3, but a maximum VOC capacity point (MVCP) exists at all locations that changes the influence of VOCs on O_3 from net production to production suppression. Analysis of individual model processes shows that more than 50% of daytime O_3 concentrations at the high-elevation rural locations (GRSM and SHEN) are transported from other areas; local chemistry is the second largest O_3 contributor. At the low-elevation location (MACA), about 80% of daytime O_3 is produced by local chemistry and 20% is transported from other areas. Local emissions (67–95%) are predominantly responsible for VOCs at all locations, the rest coming from transport. Chemistry processes are responsible for about 50% removal of VOCs for all locations; less than 10% are lost to surface deposition and the rest are exported to other areas. Metrics, such as VOC potential for O_3 production (VPOP), which links the chemistry processes of both O_3 and VOCs and MVCP, are devised to measure the different characteristics of O_3 production and VOCs. The values of the defined metrics are mapped for the entire modeling domain. Implications of this model exercise in understanding O_3 production are analyzed and discussed. Even though this study was focused on three United States national parks, the research results and conclusions may be applicable to other or to similar rural environments in the southeast United States. *INDEX TERMS:* 0345 Atmospheric Composition and Structure: Pollution—urban and regional (0305); 0368 Atmospheric Composition and Structure: Troposphere—constituent transport and chemistry; 0365 Atmospheric Composition and Structure: Troposphere—composition and chemistry; *KEYWORDS:* volatile organic compounds, ozone, measurements and modeling

[1]Now at Atmospheric Modeling Division, U.S. Environmental Protection Agency, Research Triangle Park, North Carolina, USA.

Copyright 2003 by the American Geophysical Union.
0148-0227/03/2002JD003054$09.00

Citation: Kang, D., V. P. Aneja, R. Mathur, and J. D. Ray, Nonmethane hydrocarbons and ozone in three rural southeast United States national parks: A model sensitivity analysis and comparison to measurements, *J. Geophys. Res.*, *108*(D19), 4604, doi:10.1029/2002JD003054, 2003.

1. Introduction

[2] The distribution of tropospheric ozone (O_3) has been a subject of great interest and concern not only because of ozone's deleterious effects on human health and vegetation but also because of its critical role in atmospheric chemistry. Ozone is formed from a series of photochemical reactions among its precursors, primarily nitrogen oxides (NO_x) and volatile organic compounds (VOCs), emitted from both anthropogenic and biogenic sources [*Liu et al.*, 1987; *Trainer et al.*, 1987; *Lin et al.*, 1988]. Much effort has been devoted to understanding the mechanism of O_3 production, especially in urban areas [*Trainer et al.*, 2000]. Many measurement campaigns and field studies have been conducted to help understand the chemistry and physics of tropospheric O_3 [*Apel et al.*, 1995; *Cowling et al.*, 1998; *Meagher et al.*, 1998; *Aneja et al.*, 2000a, 2000b, 2000c]. However, because of the nonlinear relationship between O_3 and its precursor species [*Lin et al.*, 1988; *Tonnesen and Dennis*, 2000a, 2000b], it is not easy to understand the mechanism leading to elevated O_3 without resorting to a model simulation. A number of air-quality models, from simple box models [*Arya*, 1999] to complex three-dimensional models, have been developed [*Morris and Myers*, 1992; *Venkatram et al.*, 1988; *Chang et al.*, 1987; *Lamb*, 1986]. A critical component of these models is how VOCs and oxides of nitrogen (NO_x) interact to produce O_3 and other oxidants. Most model mechanisms, however, were developed and verified against chamber data for relatively polluted atmosphere. Evaluation of their performance for rural conditions (especially VOC compositions) is very limited.

[3] Since passage of the 1970 Clean Air Act Amendments (CAAA), regulatory efforts to comply with the 0.12-ppmv National Ambient Air Quality Standard (NAAQS) for O_3 have proved inadequate [*National Research Council*, 1991; *Dimitriades*, 1989; *Aneja et al.*, 1999]. O_3 nonattainment continues to be a problem, especially in the southeast United States, and is attributed to the oxidation of NO_x with the presence of excessive amounts of biogenically emitted VOCs such as isoprene (ISOP) [*Trainer et al.*, 1987; *Chameides et al.*, 1988]. Nonattainment is common in southeast U.S. rural areas during summer [*Chameides et al.*, 1997; *Heck et al.*, 1984]. The new 8-hour O_3 NAAQS (0.085 ppm) is likely to bring more suburban and rural locations into noncompliance [*Chameides et al.*, 1997]. Biogenic VOCs emitted by vegetation [*Fuentes et al.*, 2000; *Fehsenfeld et al.*, 1992; *Lamb et al.*, 1993] and anthropogenic VOCs emitted by human activities are both widely present in rural areas [*Kang et al.*, 2001; *Hagerman et al.*, 1997]. Previous studies indicate that the influence of these VOCs on important aspects of atmospheric chemistry such as O_3 production can be significant [*Trainer et al.*, 1987; *Chameides et al.*, 1988; *Liu et al.*, 1987; *St. John et al.*, 1998]. Clearly, if O_3 concentrations are to be successfully controlled by implementation of control on primary pollutant emissions, the roles of both natural and anthropogenic VOCs in these rural areas must be thoroughly understood. However, our understanding of O_3 and VOC budgets in rural areas is still very limited. Emissions of biogenic VOCs as well as the roles of both biogenic and anthropogenic VOCs in O_3 production in rural areas are largely uncharacterized [*Guenther et al.*, 2000].

[4] In order to further investigate impacts of hydrocarbons and O_3 production in rural areas, this study focuses on a modeling analysis of O_3 and VOCs in three southeast United States national parks. Our previous study [*Kang et al.*, 2001] presented a comprehensive analysis of data collected from the same three parks. Even though previous studies [*Hagerman et al.*, 1997] claim that the rural areas of interest in this study are NO_x-limited for the formation of O_3, our study indicates a significant contribution from local VOCs. In order to evaluate the model, we compare model predictions with measured values. We also examine VOC emission-perturbation scenarios in the context of model process budgets to develop insights into the role of VOCs on O_3 concentrations at these rural sites.

2. Description of the Modeling System and Measurement Data

2.1. Overview of Multiscale Air Quality Simulation Platform

[5] The multiscale air quality simulation platform (MAQSIP) [*Odman and Ingram*, 1996; R. Mathur et al., manuscript in preparation, 2003] is a comprehensive Eulerian grid model that has also served as a prototype for the United States Environmental Protection Agency's (U.S. EPA) Models-3 concept [*Dennis et al.*, 1996; *Byun and Ching*, 1999]. The modeling system is configured to include detailed treatment of horizontal and vertical advection, turbulent diffusion based on K-theory, gas-phase chemical transformations using a modified version of the CBM-IV chemical mechanism [*Gery et al.*, 1989; *Kasibhatla et al.*, 1997], anthropogenic and natural emissions, dry deposition, and mixing and attenuation of photolysis rates due to the presence of clouds.

[6] In this system, temporally and spatially varying emissions of CO, VOCs, and NO_x are specified in MAQSIP. The anthropogenic emissions inventory is the ozone transport assessment (OTAG) inventory for 1995, which is in turn derived from the earlier national emissions inventory for 1990 [*Houyoux et al.*, 1996]. Biogenic emissions are calculated using the U.S. EPA Biogenic Emission Inventory System 2 (BEIS2) [*Geron et al.*, 1994].

2.2. Chemistry Mechanism

[7] The Carbon Bond Mechanism IV (CB4) used in MAQSIP is a modified version of that proposed by *Gery et al.* [1989]. Modifications reflect our increased understanding of atmospheric chemistry involving the organic peroxy radicals which form inert organic nitrates [*Kasibhatla et al.*, 1997] and isoprene chemistry [*Whitten et al.*, 1996].

[8] CB4 lumps organic species according to their carbon-bond structures. Thus hundreds of organic species are lumped into a manageable set of chemical reactions that make it feasible to simulate atmospheric processes within

Table 1. Lumping of Observed Nonmethane Hydrocarbons

Compounds	Lumped Species
Ethane	2PAR
Propene	OLE + PAR
Propane	3PAR
Isobutane	4PAR
l-Butene	OLE + 2PAR
n-Butane	4PAR
trans-2-Butene	2ALD
cis-2-Butene	2ALD2
3-Methyl-1-butene	OLE + 3PAR
Isopentane	5PAR
1-Pentene	OLE + 4PAR
n-Pentane	5PAR
trans-2-Pentene	2ALD2 + PAR
cis-2-Pentene	2ALD2 + PAR
2-Methyl-2-butene	OLE + 3 PAR
4-Methyl-1-pentene	OLE + 4PAR
Cyclopentane	5PAR
2-Methypentane	6PAR
3-Methylpentane	6PAR
n-Hexane	6PAR
cis-3-Hexene	2ALD2 + 2PAR
Methylcyclopentane	6PAR
2,4-Dimethylpentane	7PAR
Cyclohexane	6PAR
2,3-Dimethylpentane	6PAR
Toluene	TOL
n-Octane	8PAR
Ethylbenzene	TOL + PAR
m-Xylene	XYL
p-Xylene	XYL
o-Xylene	XYL
Nonane	9PAR
Isopropylbenzene	TOL + 2PAR
a-Pinene	OLE + 8PAR
n-Propylbenzene	TOL + 2PAR
1,3,5-Trimethylbenzene	XYL + PAR
b-Pinene	OLE + 8PAR
1,2,4-Trimethylbenzene	XYL + PAR
n-Decane	10PAR
Limoene	2OLE + 6PAR
Undecane	11PAR

the limits of available computing capacity. In the formulation of CB4, organic species are treated in three different ways: (1) explicitly represented species: formaldehyde (FORM), ethene (ETH), and ISOP; (2) carbon bond surrogates: one-carbon-atom surrogate paraffin (PAR), carbon-carbon double bonds surrogate olefin (OLE), and -CH_2-CHO surrogate ALD2 (acetaldehyde and higher aldehydes); and (3) molecular surrogates: TOL (monoalkylbenzene group) and XYL (dialkylbenzenes and trialkylbenzenes)[for details please refer to *Gery et al.*, 1989].

[9] For model predictions to be compared with measured values, the hydrocarbons identified in the measurements must be lumped according to CB4 mechanism. Table 1 describes a lumping procedure that follows the method of *Gery et al.* [1989] for each species identified in our previous study [*Kang et al.*, 2001].

2.3. Domain Selection of the Modeling System

[10] The modeling domain was chosen so as to adequately represent conditions at sampling sites in three national parks [*Kang et al.*, 2001]: Shenandoah National Park (SHEN), Big Meadows located at 38°31′21″N, 78°26′09″W with an elevation of 1073 m, Great Smoky Mountains National Park Cove Mountain (GRSM) located at 35°41′48″N, 83°36′35″W with an elevation of 1243 m, and Mammoth Cave National Park (MACA) at 37°13′04″N, 86°04′25″W with an elevation of 219 m. As Figure 1 shows, the domain of this modeling system consists of 34 × 42 cells using a 36-km horizontal resolution. The vertical domain varying from the surface to 100 mb is discretized using 22 layers of variable resolution; the lowest layer has a depth of 38 m. Since this study focuses on concentration field at the surface, only concentration fields at the lower 12 layers of the vertical domain are extracted from the model output.

[11] The time period for the model exercise selected is from 1200 hours on 14 July 1995 to 1200 hours on 29 July 1995 to comply with measurements that were made during July when photochemical activity was at a maximum [*Kang et al.*, 2001]. Time-varying lateral boundary conditions for various model species were derived from previous model simulations conducted over the eastern United States for the study period.

2.4. Measurement Description

[12] One-hour integrated ambient-air samples for determination of VOCs were collected (a single measurement at local noon for each day) at the three U.S. national parks described above during June through July for the year 1995. Most of the samples were collected in July at 10 m above the ground. Hourly averaged O_3 measurements during this period are also available. In the analysis of VOC samples, standards, both for retention time and quantification, were run routinely, and four internal standards were added to every chromatographic run to verify performance of the analytical system [*Farmer et al.*, 1994]. Identification of the target compounds was confirmed by mass spectrometer analysis. The method detection limit is 0.10 parts per billion carbon (ppbC), with an uncertainty of ±20%. Any target compounds not detected in the sample above 0.10 ppbC were reported as not detected (ND) and were not included in any statistical analysis. The quality of the data is further guaranteed through correlation and ratio analysis. Further details on the measurement and data analysis can be found in the work of *Kang et al.* [2001].

[13] Measured hourly concentrations of O_3 are also extracted from EPA's Aerometric Information Retrieval System (AIRS) database for the time period and domain of model simulations. There are 323 AIRS monitoring stations that have hourly O_3 concentrations within the modeling domain in 1995. When compared with the model predictions, AIRS data are averaged over all the stations which are located in the same model grid cell. Data from the monitoring locations at the three national parks are not included in the 1995 AIRS data set.

2.5. Organization of Simulations

[14] To understand the effect of VOC composition and reactivity on O_3 production, we model different emissions-perturbation scenarios for the same modeling domain. Analyses of model predictions and model process budgets from different scenarios makes clear the relative importance of different contributing factors to local O_3 concentrations at the three national parks.

[15] Table 2 gives the simulation details. Since our primary concerns in these rural areas are the characteristics of biogenic hydrocarbons represented primarily by isoprene (the contribution of terpenes to PAR and OLE can be

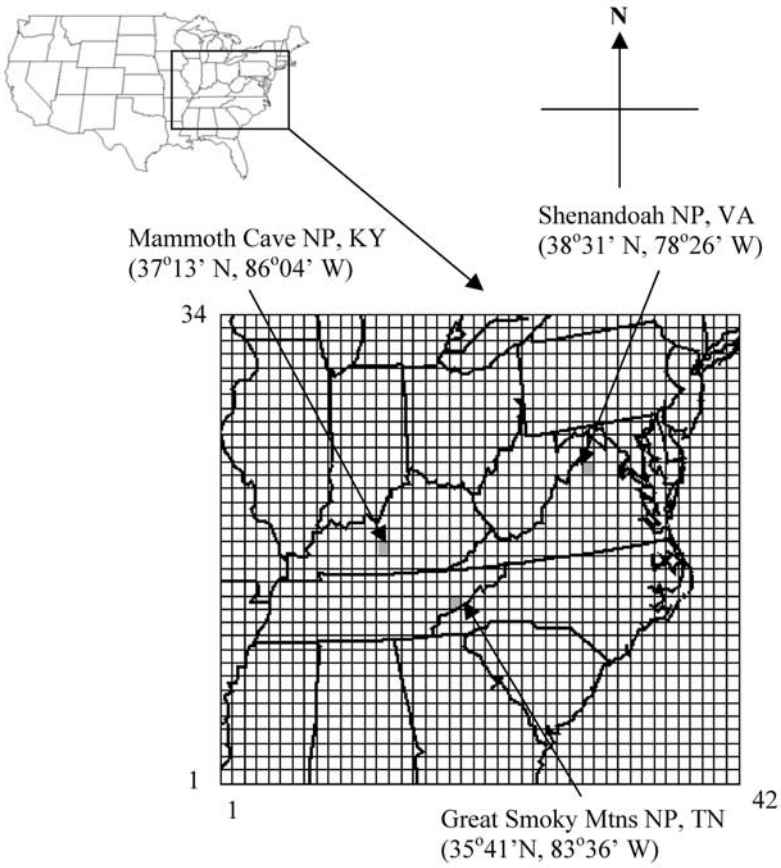

Figure 1. Map of the model domain (36-km grid size) with locations of the three monitoring sites in national parks.

neglected) in the model versus anthropogenic hydrocarbons, in the simulation design the emissions perturbation factor of isoprene is changed more often than that of other VOCs. Each simulation is assigned a name for use in the subsequent discussion. The perturbation factors represent net reduction or increase in emissions with respect to the Base Scenario designated by CS0. Further details on emissions in the Base Scenario are presented by *Houyoux et al.* [2000]. The factors are uniformly applied to all cells in the modeling domain. In CS1, emissions factors for all species are set to 0, representing effects of boundary inflow. In CS2, CS3, and CS6, emissions factors for all VOC species concerned are changed by −50, +50, and +100% to evaluate the impact of emissions variation on O_3 production. In CS4, CS5, and CS7, emissions factors are set to evaluate the effects of biogenic VOCs on O_3 production. In CS4, the emissions factors for isoprene are set to 0, while in CS5, only isoprene emissions are considered and the emissions factor is set to 1; In CS7, isoprene emissions are tripled to further assess effects of enhanced isoprene emissions. In CS8, emissions factors are set to approximately match measured values of major VOC species at the three monitoring locations.

3. Comparisons Between Measurement and Model Predictions

[16] Direct comparison between model predictions and measured values is confounded by several factors. First, the model yields grid-averaged concentrations that are dependent on the model resolution [*Tesche et al.*, 1998]; whereas

Table 2. Simulation Details and Motivations

Simulation Designation	Emissions Perturbation Factors						Motivation
	ISOP	PAR	ETH	OLE	TOL	XYL	
CS0	1	1	1	1	1	1	base scenario
CS1	0	0	0	0	0	0	assess effect of boundary inflow
CS2	0.5	0.5	0.5	0.5	0.5	0.5	assess effect of reduced emissions
CS3	1.5	1.5	1.5	1.5	1.5	1.5	assess effect of increased emissions
CS4	0	1	1	1	1	1	assess effect of anthropogenic emissions
CS5	1	0	0	0	0	0	assess effect of biogenic emissions
CS6	2	2	2	2	2	2	assess effect of doubled emissions
CS7	3	1	1	1	1	1	assess effect of increased biogenic emissions only
CS8	5	1	10	10	10	100	match the measurement

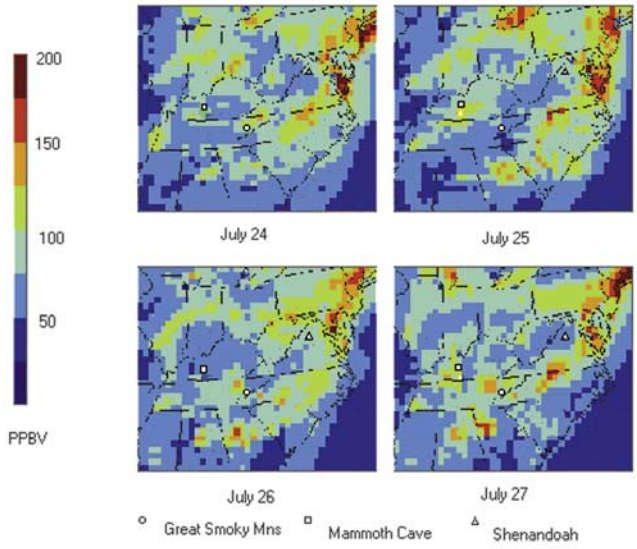

Figure 2. Model-predicted daily maximum O_3 concentrations during an episode from 24 to 27 July 1995 for the modeling domain.

individual measurements represent single-point values at the measuring locations and are easily influenced by local conditions. Second, the model lumps many organic species into small sets of manageable species for use as surrogates for real-world hydrocarbons. Third, while grid-based photochemical models represent a significant improvement over the earlier one-dimensional Lagrangian models, they have several limitations such as uncertainties in the boundary layer parameterization, representation of clouds, biogenic emissions rates, etc., which affect the proper representation of ozone and its precursors locally.

[17] Given the inherent limitations of comparing grid-averaged model predictions with point measurements and the limited frequency of available VOC measurements at these sites (one per day), the comparisons and analysis presented in the subsequent sections attempt to evaluate the mean chemical characteristics and model performance at these specific rural locations. Detailed evaluation of MAQSIP simulations of surface O_3 against EPA's AIRS data sets for the summer of 1995 can be found in the work of *Kasibhatla and Chameides* [2000] and *Hogrefe et al.* [2001a, 2001b].

3.1. Observed O_3 and Model Predictions

[18] Figure 2 presents predicted daily maximum hourly O_3 concentrations during an episode from 24 to 27 July 1995 for the modeling domain. These dates are late in the time period of the model run and thus free from the impact of model initial conditions. High O_3 levels appear each day in the east and northeast regions of this domain, e.g., the densely populated region. Daily maximum O_3 concentrations in the three national parks for this episode range from 46 ppbv (at GRSM on 25 July) to 120 ppbv (at MACA on 25 July). Back trajectory analysis shows that air flows from southwest to northeast for all three locations during this time period. Therefore the three national parks are free from the influence of high O_3 concentrations in the east and northeast regions.

Table 3. Definition of the U.S. EPA Recommended Statistical Measures

	Definition
Mean normalized bias error (MNBE)	$\frac{1}{n}\sum_{i=1}^{n}\frac{C_{\mathrm{mod}}(x,t)-C_{\mathrm{obs}}(x,t)}{C_{\mathrm{obs}}(x,t)}$
Mean normalized gross error (MNGE)	$\frac{1}{n}\sum_{i=1}^{n}\frac{\lvert C_{\mathrm{mod}}(x,t)-C_{\mathrm{obs}}(x,t)\rvert}{C_{\mathrm{obs}}(x,t)}$
Unpaired peak prediction accuracy (UPA)	$\frac{C_{\mathrm{mod}}(x,t)_{\max}-C_{\mathrm{obs}}(x,t)_{\max}}{C_{\mathrm{obs}}(x,t)_{\max}}$
Correlation coefficient (R)	$\frac{\frac{1}{n}\sum_{i=1}^{n}\left[\left(C_{\mathrm{mod}}(x,t)-\overline{C_{\mathrm{mod}}}\right)\left(C_{\mathrm{obs}}(x,t)-\overline{C_{\mathrm{obs}}}\right)\right]}{\frac{1}{n}\sum_{i=1}^{n}\left[\left(C_{\mathrm{mod}}(x,t)-\overline{C_{\mathrm{mod}}}\right)^2\right]^{0.5}\times\frac{1}{n}\sum_{i=1}^{n}\left[\left(C_{\mathrm{obs}}(x,t)-\overline{C_{\mathrm{obs}}}\right)^2\right]^{0.5}}$

[19] In order to evaluate air quality model performance, the U.S. EPA stipulated the application of statistical measures listed in Table 3 to predicted ozone concentrations [*United States Environmental Protection Agency* (*U.S. EPA*), 1991]. Observation-prediction pairs are often excluded from the analysis if the observed concentration is below a certain cutoff; the cutoff levels varied from study to study but often a level of 40 or 60 ppb is used [*Russell and Dennis*, 2000; *Hogrefe et al.*, 2001a, 2001b]. Although there is no objective criterion set forth for a satisfactory model performance, U.S. EPA suggested values of 5–15% for the mean normalized bias error (MNBE), 15–20% for the unpaired peak prediction accuracy (UPA), and 30–35% for the mean normalized gross error (MNGE) to be met by modeling simulations being used for regulatory applications. The values for the MNBE and UPA can be either positive or negative. The results of model performance evaluation using the U.S. EPA recommended statistical measures (with a cutoff of 40 ppb and 15 days of AIRS data and model predictions) for the three national parks are presented in Table 4. Only the MNBE value at MACA moderately exceeds the U.S. EPA suggested values of 5–15%. And also note that all the MNBE values are positive, implying that the model systematically overestimates O_3 concentrations. The MNGE values are all within the U.S. EPA suggested values of 30–35%. The UPA values indicate that the peak O_3 concentrations are underpredicted at GRSM and SHEN by about 5% but overpredicted at MACA by 9.5%. The correlation coefficients (R) ranging from 0.6538 to 0.7089 for the three sites indicate that the model can capture O_3 variation pattern reasonably well.

[20] Figure 3 presents a scatterplot of model predicted (Base Case CS0 and CS8) versus observed O_3 concentrations from AIRS for the three model cells in which the three monitoring locations are located. For convenience of comparison, the linear fitted line, 1:1 line, 2:1 line, and 1:2 line are also plotted on the plot to indicate the scattering range. Figure 3 shows that when observed O_3 concentrations (CS0) are less than 40 ppbv, the model tends to overestimate, with

Table 4. U.S. EPA Recommended Evaluation Statistics for Ozone Predictions

	Site		
Statistics	GRSM	MACA	SHEN
MNBE	3.0%	19.1%	9.0%
MNGE	22.9%	28.8%	22.0%
UPA	−5.9%	9.5%	−5.1%
R	0.6534	0.6769	0.7089

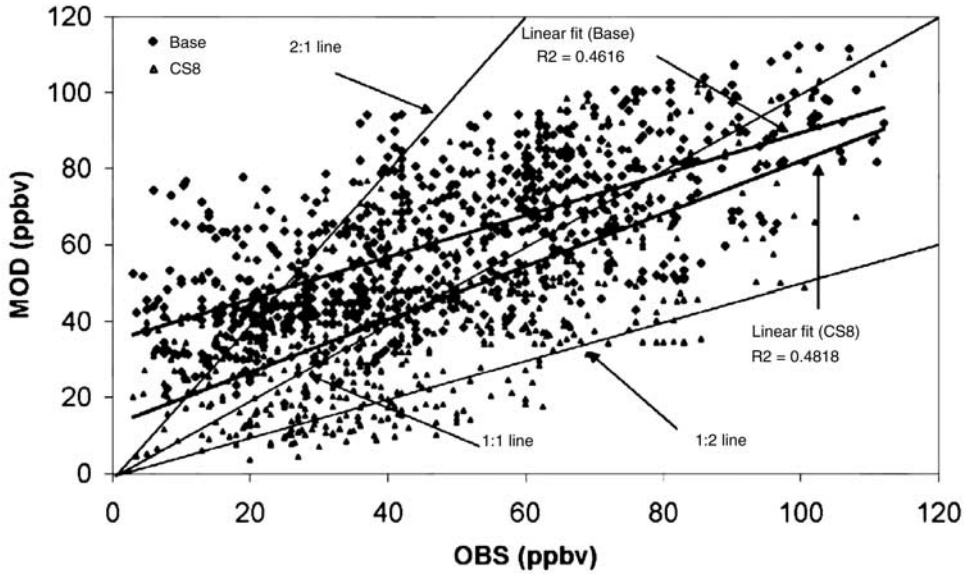

Figure 3. Scatterplot of model predicted (MOD) versus observed (OBS) O_3 concentrations for all three national parks.

significant number of points beyond the 2:1 line. When the observed O_3 concentrations are greater than 40 ppbv, all the points scatter around the 1:1 line and all points are within a factor of 2 in both directions. This is the rationale by which the cutoff value is selected at 40 ppbv when we calculate the statistical metric. Compared with the Base Case, CS8 tends to predict lower O_3 concentrations that are in better agreement with observed values, especially when O_3 concentrations are low.

[21] Figure 4 presents diurnal variations of O_3 concentrations of model predicted and measured values from both the three national parks and AIRS data within the grid cell containing the national park sites averaged over the modeling period for each hour. At GRSM, predictions and measured values are in good agreement during daytime with slight difference during nighttime. At SHEN, predictions are in better agreement with measured values from the national park than with AIRS data except for the midday period (1000–1700 hours). At GRSM and SHEN, the two high-elevation locations, diurnal changes in measured values are quite small or insignificant and the model seems to capture this pattern reasonably well. The daily averaged values of both predicted and measured at the parks are almost the same (for instance, at SHEN, 61.03 and 60.70 ppbv, respectively). The significant diurnal cycle of AIRS data at SHEN is due to the fact that there are only a few low-elevation urban locations included. However, the situation at MACA is quite different. Both model predictions and measured values have a significant diurnal variation with higher values during daytime and lower values during nighttime. The model tends to overestimate both daytime and nighttime values, with a larger margin during nighttime. The predictions more closely match measured values from AIRS data than those at the park in both variation pattern and magnitude. The measured values at the park show significant diurnal variations with very low values during night (only a few ppbv that is even lower than O_3 levels in clean atmosphere). The low concentrations of O_3 are likely caused by low nighttime inversion in the river valley and nighttime deposition [*Altshuller*, 1986]. Clearly, model resolution is not fine enough to simulate the situations at this specific location.

3.2. Observed VOCs and Model Predictions

3.2.1. Concentrations

[22] Figure 5 shows the time series of both model predicted and observed concentrations for 6 model species at different locations. The observed values stand for hourly integrated mean concentrations from 1200 to 1300 LT, and the model predictions are the mean concentrations at hour 1200 and 1300 (LT) on the same days when observations are available. Listed simulation scenarios are CS0 (Base Scenario), CS3 (factor = 1.5), CS6 (factor = 2), CS7 (ISOP factor = 3, the rest 1), and CS8 (factors: ISOP 5, PAR 1, XYL 100, and all the others 10). Except CS0, all the other simulation scenarios have increased VOC emissions compared with CS0. At all locations, the Base Scenario (CS0) significantly underpredicts isoprene concentrations. The observed isoprene concentrations are between the values predicted by CS7 and CS8 except the one on 23 July at GRSM; it is a good match between observed concentrations and the predicted values by CS8 at MACA even though most of the observed concentrations are still higher than the predicted ones by this scenario; however, at SHEN, the observed isoprene concentrations match the predicted values by CS7 better than any other scenarios. In general, the Base Scenario underpredicts isoprene concentrations with a factor of about 3–5 at the three locations. As *Guenther et al.* [2000] points out, a factor of 3 is probably a reasonable estimate of the uncertainty associated with annual biogenic emissions for the contiguous United States, but predictions for specific times, locales, and compounds can be much more uncertain. The lower isoprene predictions may be attributed to three possible effects: (1) biogenic hydrocarbons emissions for this area are probably underestimated; (2) model resolution is not fine enough to adequately

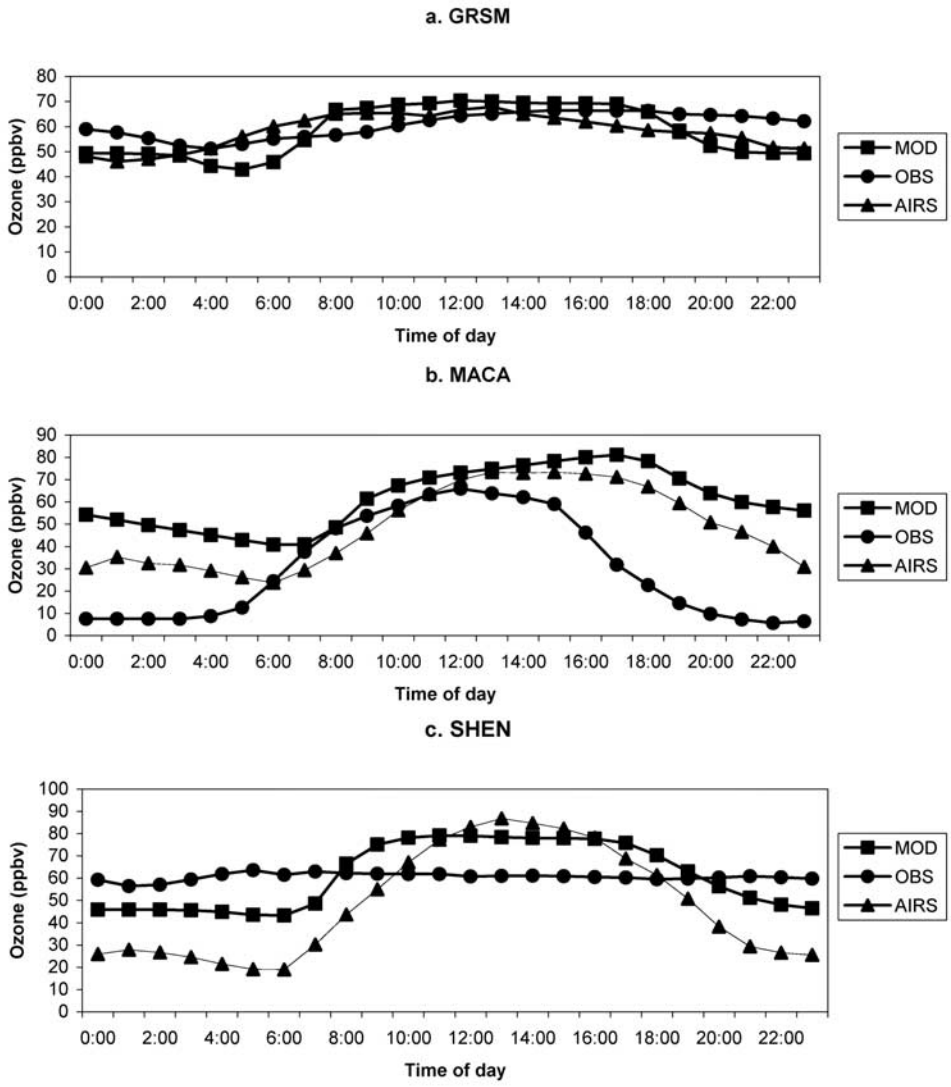

Figure 4. Model-predicted and observed average diurnal variations of O_3 concentrations. MOD, model predictions; OBS, observed values at the parks; AIRS, data from EPA's AIRS data set.

simulate the complex terrain effects; (3) reactivity of isoprene makes its spatial distribution more uneven.

[23] As Figure 5 shows, the model predicted and observed distributions of anthropogenic VOC concentrations vary both in species and in location (anthropogenic species are not shown for SHEN because anthropogenic VOCs are considered to be contaminated at this site in 1995; see *Kang et al.* [2001]). The single-bonded one atom surrogate, PAR, is the species whose predictions have closer agreement with observations compared to the other species, and the difference between predications and observations are within a factor of 2 at GRSM and within a factor of 2 for more than half of the points and a factor of 3–5 for the rest at MACA (the largest increase in PAR emissions is a factor of 2). The Base Scenario significantly underpredicts all anthropogenic species except PAR. However, an increase by a factor of 10 (CS8) for ETH seems too high at GRSM, but reasonable at MACA. The predictions for OLE by CS8 are a good match at GRSM but are still too low at MACA for 4 of the 12 data points. Notice that the variation pattern of PAR is very similar to OLE at MACA and the higher concentrations on 19–22 July may be indicative of local pollution events. The molecular surrogate TOL is overpredicted by CS8 at GRSM, but it is a good match at MACA. Even though the predictions of XYL in the Base Scenario are almost 100 times lower than observations, a systematic increase in XYL emissions throughout the domain by a factor of 100 seems too high compared to the observed values.

[24] Through the above analysis, it is apparent that the daily averaged base O_3 predictions are comparable with the measured values, with a tendency to overpredict during the daytime and underpredict at night. However, measured isoprene values are generally higher than base predictions by a factor of 3–5. Besides O_3, PAR is the species whose base predictions have closer agreement with measured values compared to the other species. This is because PAR mostly consists of anthropogenic hydrocarbons, which are less reactive under normal conditions than other species, and hence PAR is more evenly distributed spatially. For all

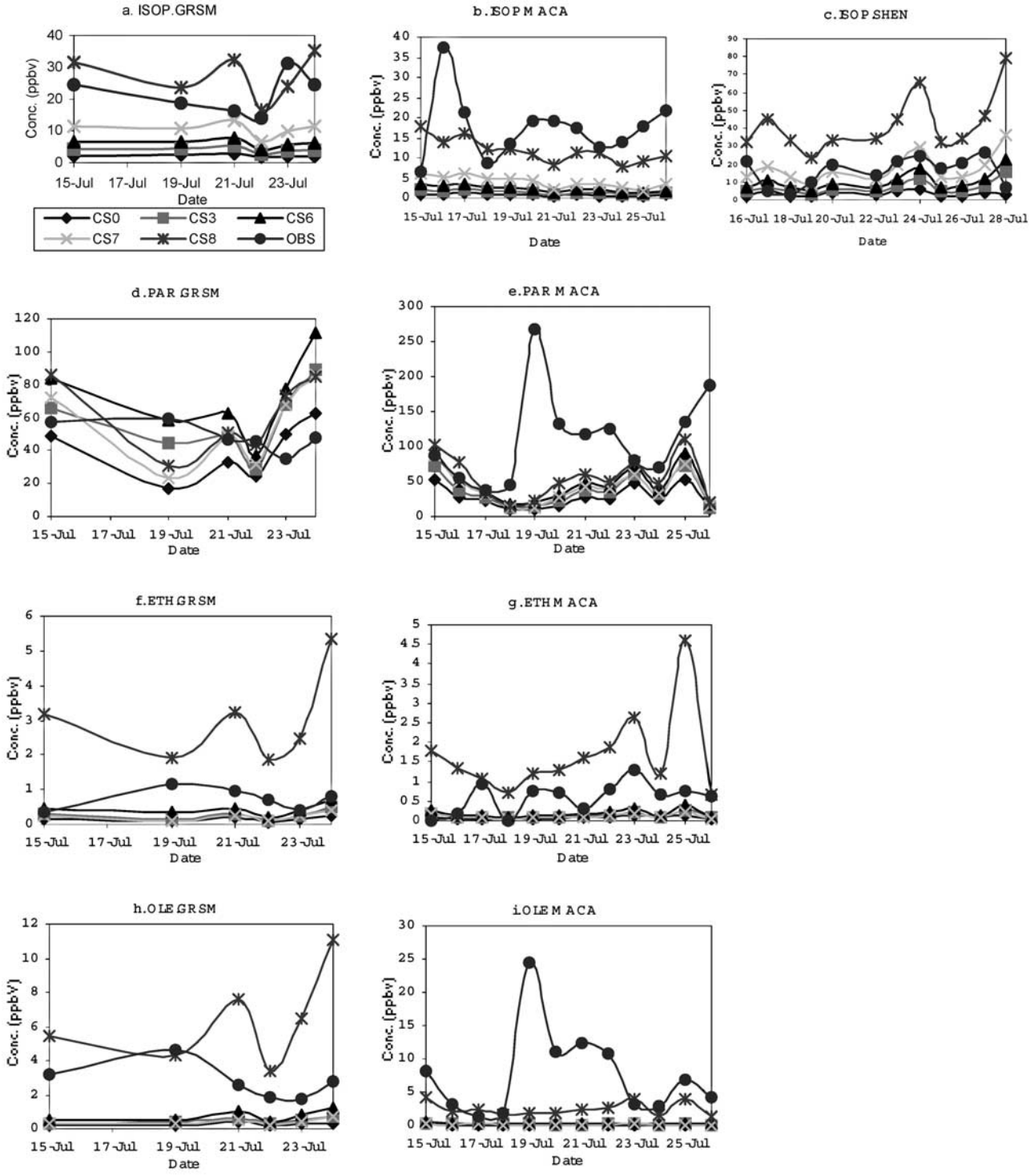

Figure 5. Time series of model-predicted and observed lumped species. CS0, CS3, CS6, CS7, and CS8 are simulation scenarios and OBS is observation. The title of each figure contains the name of the lumped species and the name of the location separated by a dot.

other species, including ETH, OLE, TOL, and XYL, the base model predictions are much lower than measured values. All of these are composed of mainly reactive anthropogenic hydrocarbons, whose higher measured values may indicate the influence of local sources which are not adequately resolved by the model. The discrepancy may also be attributed to the inaccuracy of the emissions inventory of organic species used by the Base Scenario as *Henry et al.* [1997] reported and to the intrusion of the emissions of the Canadian wildfires during the modeling period as reported by *McKeen et al.* [2002]. Furthermore, the 36 km $\times$ 36 km grid-averaged values may not represent

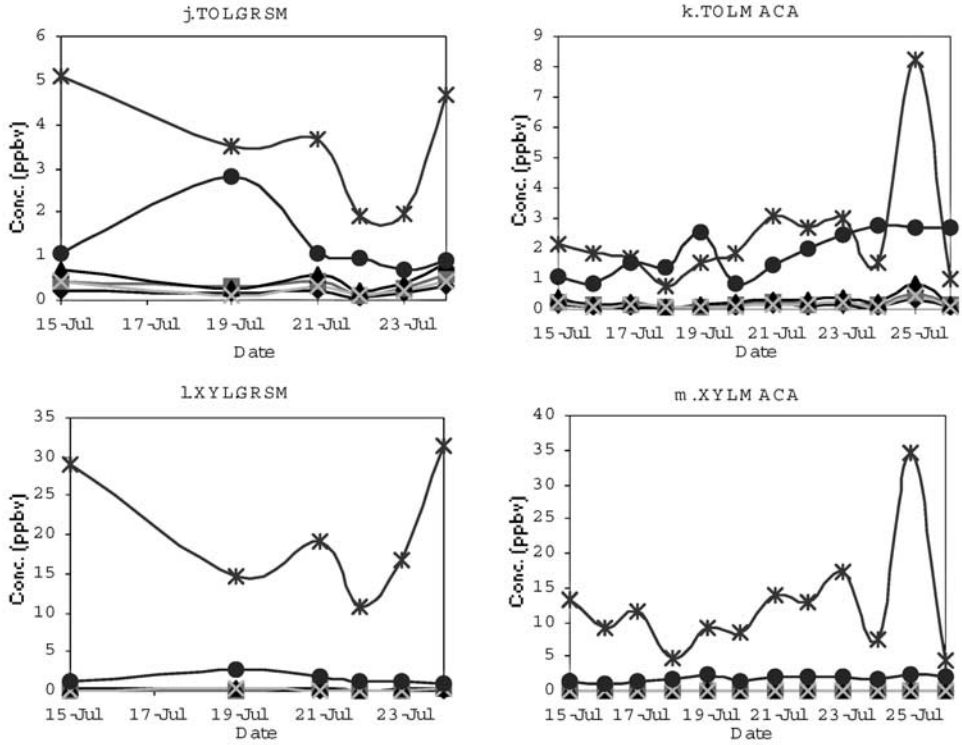

Figure 5. (continued)

the point measurements. The comparison of predictions with limited available VOC measured values at these sites indicate that though the model does not capture the absolute concentrations of individual VOC species when paired in space and time, the predicted values are within the measured diurnal variation range at these sites.

3.2.2. Reactivity

[25] An important aspect of the role of VOCs in atmospheric chemistry is their individual reactivity. The relative importance of any VOC species in oxidant chemistry is limited by its rate of reaction with OH to produce highly reactive organic peroxy radicals (RO_2). Since the reactivity of individual species may vary by orders of magnitude, a concentration-based analysis may not always indicate the relative importance of a VOC species because a relatively abundant species may not be as reactive as other less-abundant species. On the other hand, comparing predictions of the relative reactivity of each species with measured values may provide valuable information about model performance.

[26] *Mathur et al.* [1994] define a reactivity-weighted organic (RWOG) based on the typical reaction between a VOC species (relative humidity, RH) of concentration C_j and OH,

$$\text{(R1)} \qquad \text{RH} + \text{OH} \rightarrow \text{R}\cdot + \text{H}_2\text{O}$$

as

$$\text{RWOG} = \sum_{j}^{N} \text{K}_{\text{OH}}(j) C_j, \qquad (1)$$

where N is the number of organic classes (explicit compounds and generalized reactivity classes) in the chemical mechanism and $\text{K}_{\text{OH}}(j)$ is the rate constant of the reaction between OH and the organic species (j), taken at 298°K. Figure 6 presents the relative contributions of various VOC species to RWOG (here RWOG includes ethene, isoprene, PAR, OLE, TOL, and XYL) for both model predictions (Base Case, midday values) and measured values at GRSM and MACA. In general, both predictions and measured values share the same variation pattern across all the species and are comparable for each species at both locations. The mean fractional contributions

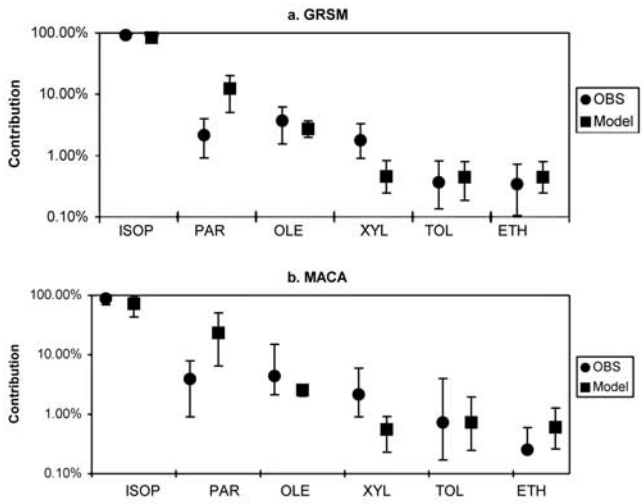

Figure 6. Fractional contributions of various hydrocarbons to total organic reactivity (RWOG). The vertical bars are the range of maximum and minimum contributions.

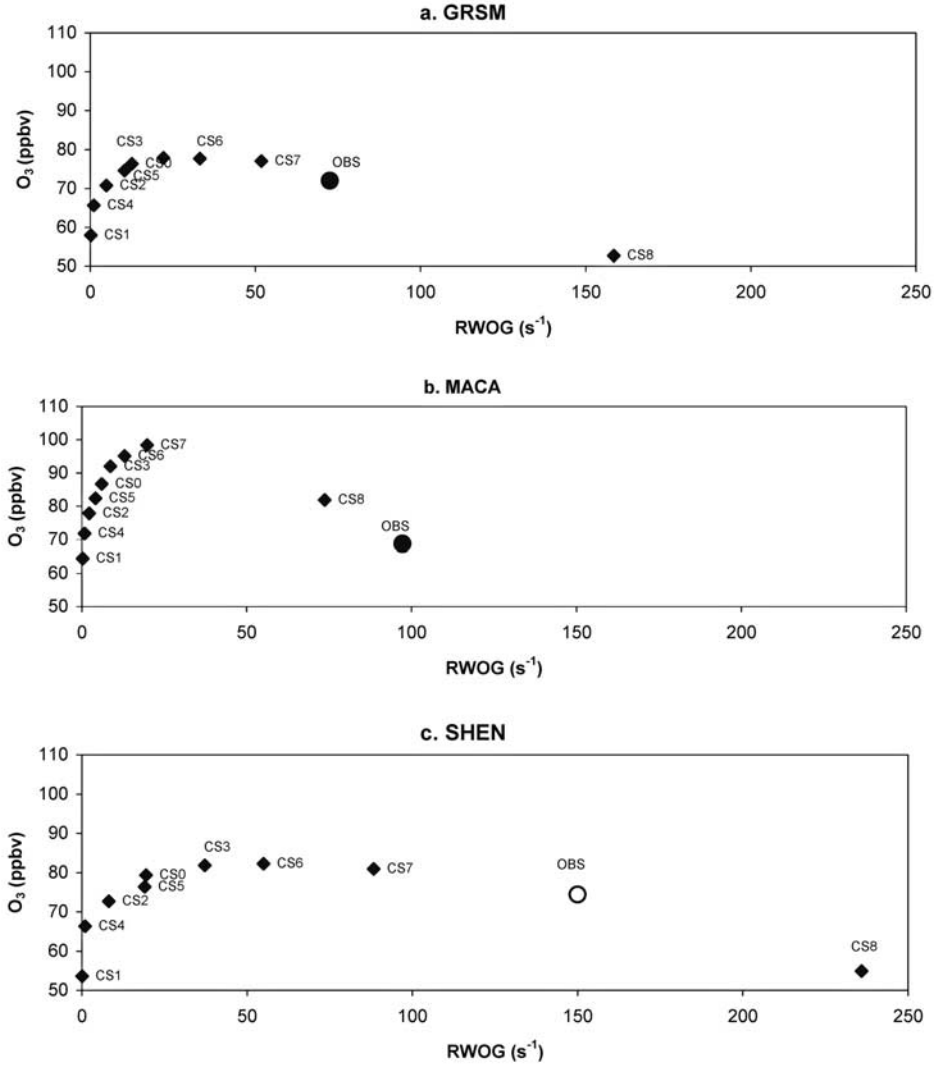

Figure 7. Variations of mean daily predicted and observed maximum O_3 concentrations with RWOG. OBS is observation. At SHEN the observed RWOG that is represented by an open circle is an estimated value based on isoprene and other hydrocarbons due to considered contaminations to anthropogenic hydrocarbons.

of isoprene to RWOG for both predictions and measured values are more than 75% (at GRSM, the mean contribution for the measured value is 91.6%, and that for the prediction is 83.5%; at MACA, the values are 88.5 and 74.7%). As Figure 6 indicates, the predicted fractional contribution of PAR is about five times greater than the measured values at both sites (even though the predicted PAR concentrations match the observed values within a factor of 2 (Figure 5), the predicted fractional contribution of PAR to RWOG is much higher than observed value due to the lower predicted RWOG). But measured OLE and XYL fractional contributions to reactivities are slightly greater than prediction. The measured and predicted fractional contributions for TOL and ETH at both locations are not significantly different; all are less than 1%. In any case, the fractional reactivity contributions from isoprene and PAR combined exceed 95% of the total aggregated reactivity. These results indicate that even though the model does not capture the midday concentrations for each individual VOC species, it captures their relative contributions to the total VOC reactivity. One should be aware, however, that model resolution [*Tesche et al.*, 1998], lumping procedure, and accuracy of the emissions data may influence these results.

4. Sensitivity of O_3 Production to VOCs and Process Analysis

4.1. Ozone Concentrations in Different Scenarios

[27] Figure 7 presents variation of mean daily maximum O_3 predictions with RWOG for different scenarios at the three locations. For comparison, the measured values are also shown. As expected, the scenario (CS1) in which emissions for all VOC species are set to 0 gives the lowest O_3 concentrations at all three locations. As VOC emissions factors increase from 0 to 2.0 (CS1, CS2, CS0, CS3, and

CS6), the daily maximum O_3 prediction also increases, but nonlinearly. From CS1 to CS2, the increment plays a larger role than it does from CS2 to CS0; that is, the increment from 0 to 0.5 VOC plays a larger role than that from 0.5 to 1.0 VOC. There is no significant change in O_3 concentration when the VOC emission factor further increases to 1.5 and 2.0, especially at GRSM and SHEN. CS5 (in which only isoprene is emitted; factor = 1) and CS0 (Base Scenario) predict very similar daily maximum O_3 concentrations, indicating that isoprene plays a major role (>90%) in O_3 production in these locations. However, CS1 (no VOCs) and CS4 (no isoprene but other VOCs = 1) show that O_3 production is still significant (mean daily maximum concentrations increased by 7–11 ppbv). This implies that, when isoprene is absent, other VOC species contribute significantly to O_3 production (on average, isoprene emissions rates are 2–4 times higher than other VOCs at the three locations). As Figure 7 indicates, in CS8, daily maximum O_3 predictions are significantly reduced compared to other scenarios at all three locations, and of different magnitude at each location. The mean daily maximum O_3 prediction at GRSM is 5.2 ppbv lower than predicted by CS1, and 15.6 ppbv (20.4%) lower than CS0. This signifies that, at this level of VOC emissions, O_3 production is suppressed by the presence of extra VOCs. The observed values at the three locations fit well on the simulated trends except that the RWOG value is only the best estimated value based on isoprene and other hydrocarbons because PAR and OLE are considered contaminated, as mentioned above. In terms of RWOG at the three locations, the observed values are somewhere around the model predictions in the scenarios 7 and 8, and this further proves *Henry et al.* [1997]'s observation that the emissions inventory of organic species used in the model Base Scenario is indeed lower than observed values.

[28] In a field study for VOCs and O_3 in a suburban area of North Carolina, M. Das et al. (Vertical distribution of VOCs and ozone observed at suburban North Carolina and estimation of OH-densities from vertical profile, submitted to *Journal of Atmospheric Chemistry*, 2003, hereinafter referred to as Das et al., submitted manuscript, 2003) also observed that O_3 is produced at lower levels of VOCs (<60 ppbC) but destroyed at higher levels. In the literature, the ozone-production mechanism is often illustrated using ozone isopleths [*Dodge*, 1977]. When the ratios of nonmethane hydrocarbon (NMHC, the sum of model species PAR, OLE, TOL, XYL, ETH, and ISOP for this study) to NO_x are larger than certain values (15:1 in the empirical kinetic-modeling approach), the maximum O_3 concentration is not very sensitive to the hydrocarbon concentrations. As Table 5 indicates, except for CS1, the NMHC/NO_x ratios for all other scenarios, including the Base Scenario, at all the three locations are within the NO_x-limited region on the ozone isopleths. *Tonnesen and Jefferies* [1994] show through ozone-isopleths diagrams that within the NO_x-limited region, O_3 production decreases slightly as VOC increases due to increased reaction of RO_2 with NO_2 to produce stable nitrogen products that result in fewer NO-to-NO_2 conversions per initial NO_x. In the CB4 mechanism [*Gery et al.*, 1989], two universal peroxy radical operators, XO2 and XO2N, are used as surrogates for organic peroxy radicals that are produced by the oxidation

Table 5. Averaged Daytime NMHC/NO_x Ratio (ppbv/ppbv) Over Entire Model Period[a]

Scenario	GRSM	MACA	SHEN
CS0	118.73	18.49	58.24
CS1	9.66	4.00	1.48
CS2	60.70	10.85	27.88
CS3	176.58	26.51	88.96
CS4	62.69	11.59	25.99
CS5	54.87	9.98	27.04
CS6	233.34	34.67	119.67
CS7	201.88	31.48	108.75
CS8	361.00	61.19	212.81

[a]NMHC, nonmethane hydrocarbons, is the sum of model species PAR, OLE, TOL, XYL, ETH, and ISOP.

of anthropogenic and biogenic hydrocarbons, mainly including the following reactions

$$\text{(R2)} \qquad \text{ISO3} + \text{NO} \rightarrow \text{ISN}$$

$$\text{(R3)} \qquad \text{ISO4} + \text{NO} \rightarrow \text{ISN}$$

$$\text{(R4)} \qquad \text{ISNT} + \text{NO} \rightarrow \text{DISN}$$

$$\text{(R5)} \qquad \text{MV1} + \text{NO} \rightarrow \text{MVNT}$$

$$\text{(R6)} \qquad \text{BZO2} + \text{NO}_2 \rightarrow \text{PBZN}$$

$$\text{(R7)} \qquad \text{PHO} + \text{NO}_2 \rightarrow \text{NPHN}$$

$$\text{(R8)} \qquad \text{CRO} + \text{NO}_2 \rightarrow \text{NCRE},$$

where ISO3 and ISO4 are isoprene O-adducts, ISN and ISNT are nitrates of isoprene, DISN is dinitrate of isoprene, MV1 is methylvinyl ketone OH-adduct, MVNT is methylvinyl ketone nitrate, BZO2 is peroxybenzoyl radical, PBZN is peroxybenzoyl nitrate, PHO is phenoxy radical, NPHN is nitrophenol, CRO is methylphenoxy radical, and NCRE is nitrocresol.

[29] Reactions (R2)–(R5) are isoprene reactions, and reactions (R6)–(R8) are reactions for aromatic surrogate TOL. The typical rate constants for all these reactions are in the range of $\sim 10^{-11}$–10^{-12} cm^3 molecule^{-1} s^{-1}, which are comparable to most of the VOC and OH reactions and inorganic reactions of NO and NO_2. All these nitrate compounds formed in these reactions are stable under normal atmospheric conditions and may be eventually removed through gas and/or aerosol deposition. Model results show that with the increase of VOCs (primarily ISOP) the mean reduction of NO is from 38% (CS3) to 68% (CS8) and the mean reduction of NO_2 is from 12% (CS3) to 35% (CS8) for the three locations studied. Correspondingly, the surrogate operators XO2N and XO2 increase from 91% (CS3) to 165% (CS8) and from 83% (CS3) to 182% (CS8), respectively. The significant reduction of NO_x due to increased VOC concentrations (especially ISOP) is the

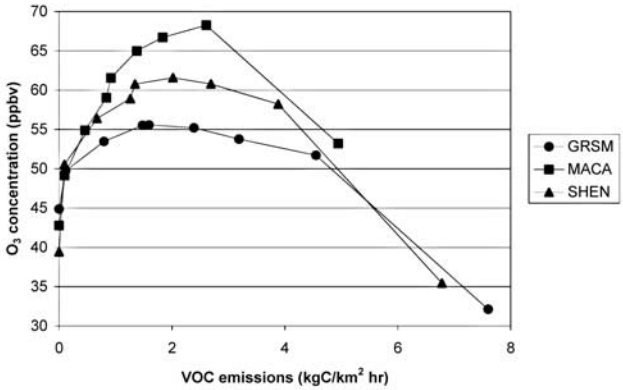

Figure 8. Variations of mean O_3 concentrations with mean VOC emissions. Note that both O_3 concentrations and VOC emissions are averaged over the whole modeling period for each scenario.

primary reason of reduced O_3 production at higher VOC (primarily ISOP) emissions. However, in NO_x-rich environment, this effect is not significant. Only when the reduction of NO_x reaches the level where O_3 production is dependent on NO_x availability does this effect become significant, such as at GRSM and SHEN.

[30] If the modified CB4 mechanism [*Gery et al.*, 1989; *Kasibhatla et al.*, 1997] is meant to imply hydrocarbon/O_3 chemistry, then O_3 is indeed reduced by increasing certain hydrocarbons under certain conditions. It must be noted that the emissions factors in CS8 are chosen arbitrarily for all the cells in the modeling domain based solely on analysis of the measured values at the three locations; even for the three locations, each has its own unique characteristics for each VOC species, and the designated emissions factors are only an approximation.

[31] Figure 8 shows the relationship between mean predicted O_3 concentrations and mean VOC emissions for the entire modeling period (both are averaged for each scenario and each point on the figure corresponds to a scenario). It is obvious that VOC emissions have significant influence over O_3 concentrations at each location, and all plots have maximum points.

[32] If we define maximum VOC capacity point (MVCP: the point where any addition of VOCs reduces O_3 concentrations) as

$$\text{MVCP} = \text{VOC emission}\left(\text{kgC/km}^2\text{h}\right) \text{ when} \frac{d[\text{O}_3]}{d[\text{VOC}]_e} = 0, \quad (2)$$

where $[O_3]$ is O_3 concentration, and $[VOC]_e$ is VOC emissions (kg C/km^2 h), then the MVCPs are 1.59 (GRSM), 2.61 (MACA), and 2.02 (SHEN) kg C/km^2 h. MVCP may be interpreted for the fixed NO_x emissions level of the Base Scenario to mean that O_3 concentrations increase with the increasing VOC emissions before this point, and decrease after that point. In the decrease phase, O_3 production is inhibited by the lack of NO_x. For the Base Scenario, only the conditions at GRSM can be considered to be NO_x-limited in terms of O_3 production as other studies have suggested because O_3 production has reached its maximum with regard to VOC emissions (its MVCP point has the same emissions as the Base Scenario). Both MACA and SHEN in the Base Scenario have not reached their MVCPs, so any additional VOC emissions at these two locations may increase O_3 concentrations.

[33] To put the three national parks into perspective, Figure 9 gives the relative MVCP (RMVCP) values for the entire modeling domain. RMVCP is defined as the difference between the MVCP and the VOC emissions rate at Base Scenario. RMVCP can be positive, zero, or negative. A positive value indicates that the MVCP point is reached at an emission level greater than the Base Scenario; a zero value indicates that the MVCP is just the emission level of the Base Scenario; and a negative value indicates that the MVCP has been reached before the emissions level reaches that of Base Scenario. If the emission rate of the Base Scenario for both NO_x and VOCs reflects the reality, then a negative or zero RMVCP indicates that O_3 production at this location (blue and some of the green areas in Figure 9) is limited by the availability of NO_x. In Figure 9, MVCP points are never reached for the regions shaded red within the emissions perturbation schemes devised in this study. The regions are usually urban locations such as New York and Chicago areas where there are large NO_x emissions and locations over sea where little VOC emissions exist. In these regions, VOCs are highly productive to produce O_3 (NO_x is also productive in the locations over sea due to its low concentrations). The implication of Figure 9 is that in the blue or green regions the effective way to control O_3 is to reduce NO_x emissions. As discussed earlier, the actual measured VOC concentrations are higher than the predicted by the model Base Case in the three national parks, thus O_3 production in these areas is all in the negative RMVCP region. It seems that the effective way to

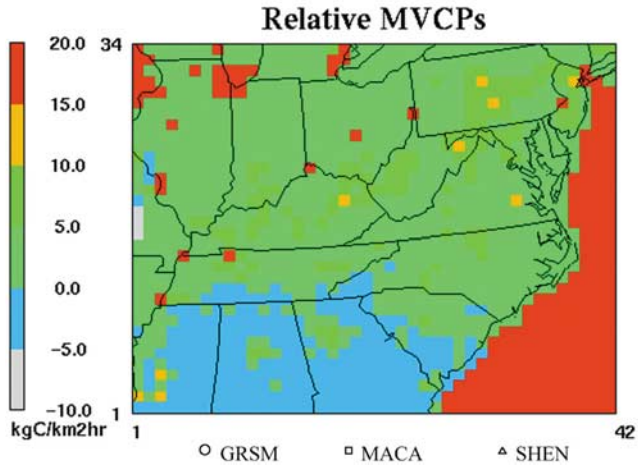

Figure 9. Map of mean relative MVCP (RMVCP). Relative MVCP = The MVCP point defined in the text, VOC emissions in Base Scenario. Positive values indicate that with increase of VOC emissions above Base Scenario, O_3 concentration will increase. Negative values indicate that the MVCP point has been reached before the emissions level for Base Scenario and at the Base Scenario emissions rate, O_3 concentration has decreased. The MVCP points are never reached within the designed emissions perturbation scheme in the red areas. VOCs are highly productive in these areas. Plenty of NO_x exist to assist VOCs in producing O_3.

reduce O_3 in these national parks is to reduce NO_x. However, since NO_x concentrations are already low at the two high-elevation locations (GRSM and SHEN), except at MACA O_3, concentrations can be reduced by the reduction of NO_x emissions; it is not an effective way to reduce O_3 production at GRSM and SHEN by reducing NO_x. As we will see in the following discussion, local production is less than half of the O_3 budget at GRSM and SHEN, thus any local control strategy may not be effective.

[34] As discussed earlier, when using ozone isopleths, if VOC is increased within NO_x-limited area, O_3 concentration usually levels off, but it is not predicted to decease as suggested by the MVCP. However, at all the three park locations and in other regions in Figure 9, our analysis strongly signifies the existence of MVCP, and it is suggested by observations (Das et al., submitted manuscript, 2003). This implies that the conditions under which O_3 isopleths are obtained are different from the conditions in this study. As already discussed, highly reactive VOCs (especially isoprene) help reduce NO_x concentrations, which under NO_x-scarce environment suppresses O_3 production.

4.2. Process Budgets

[35] In the MAQSIP model each of the physical and chemical processes is cast into modules following the time-splitting approach. Each process module operates on a common concentration field, making it possible to analyze budgets of modeled species by examining the contribution from each modeled process. In this study, we analyze model budgets in terms of various physical/chemical processes such as chemistry, horizontal and vertical advection, horizontal and vertical diffusion, dry deposition, and emissions based on the Base Scenario (CS0). Not all of these processes can be equally weighted in the budgets of ozone and different VOC species. The vertical budget of each process (Bi) is the weighted contribution from each layer and is calculated as follows:

$$\mathrm{Bi} = \frac{\sum_{j=1}^{N} (\sigma_{j-1} - \sigma_j) C_j}{\sum_{j=1}^{N} (\sigma_{j-1} - \sigma_j)}, \qquad (3)$$

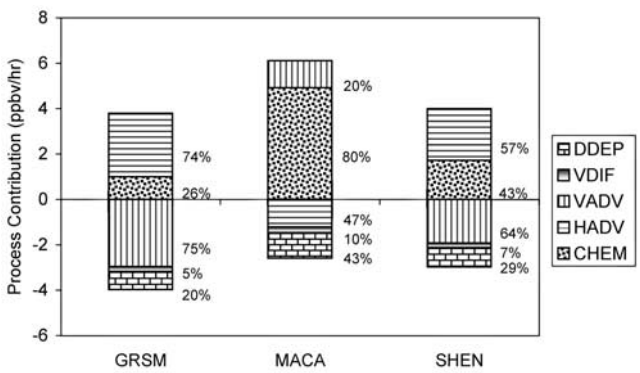

Figure 10. Model O_3 budgets over entire modeling period averaged for the photochemically active period of the day (1000–1700 hours). DDEP, deposition; VDIF, vertical diffusion; VADV, vertical advection; HADV, horizontal advection; CHEM, chemistry.

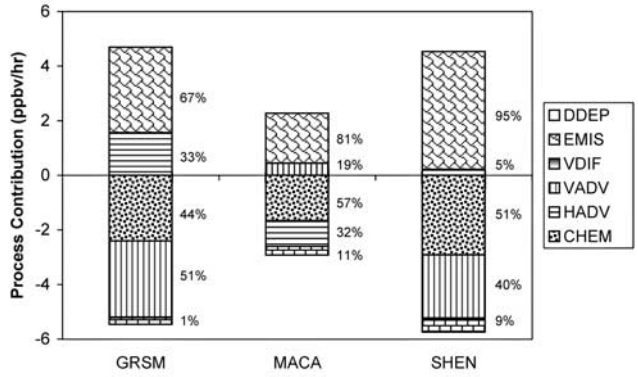

Figure 11. Mean VOC budget over entire modeling period for the photochemically active period of the day (1000–1700 hours). DDEP, dry deposition; EMIS, emissions; VDIF, vertical diffusion; VADA, vertical advection; HADV, horizontal advection; CHEM, chemistry.

where σ represents the vertical coordinate system, σ_j is the boundary σ value of the jth layer, C_j is the contribution of the process (ppbv/h) at jth layer, and N is the number of vertical layers (N = 12 in this calculation).

4.2.1. Modeled Ozone Budgets

[36] Five processes, chemistry, horizontal advection, vertical advection, vertical mixing, and deposition, have a significant effect on modeled O_3 budgets in this modeling study. Figure 10 presents the average contributions of each process to the modeled daytime O_3 budget across the modeling period as well as the whole vertical modeling domain for each location. For all locations, both chemistry and horizontal advection contribute to the local O_3. Also, note that positive contribution (accumulation) is not balanced by negative contribution (removal) at each location, especially at MACA where O_3 accumulation is much higher than its removal. The difference between accumulation and removal reflects the average net O_3 production or destruction at the location. For instance, there is an average net O_3 production rate of 3.52 ppbv/h at MACA, but an average net O_3 destruction rate of 0.18 ppbv/h at GRSM.

4.2.2. Modeled VOC Budget

[37] Figure 11 shows VOC budgets for each location. Six processes are included: chemistry, emissions, horizontal advection, vertical advection, vertical diffusion, and dry deposition This budget picture indicates that even for these rural locations, local emissions account for most of the VOC concentrations and the impact of long-range transport plays only a smaller role in regulating the local VOC concentrations. Unlike O_3 budgets, the positive and negative contributions for VOC budgets are almost balanced at all locations.

4.3. Chemistry Processes

[38] Chemistry processes are important to both O_3 and VOCs local budgets in the areas studied. Even O_3 transported to the area is also produced through photochemistry processes somewhere in the atmosphere. VOCs are predominantly emitted locally and about half consumed by chemistry and about 33–50% exported to other areas. Most of the exported VOCs are removed by various chemistry and photochemistry processes sooner or later. Therefore it is necessary to further

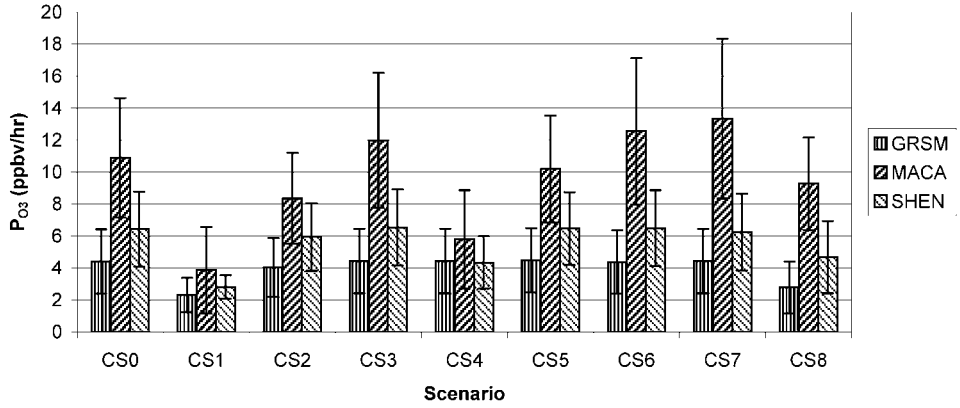

Figure 12. Model-predicted mean daytime O_3 production by chemistry (P_{O_3}). Daytime O_3 production is the average of hourly O_3 production from 1000 to 1700 hours on the day.

analyze the chemistry processes. The magnitude of O_3 chemistry budget represents the net ozone produced through local photochemical processes. During the photochemically active period of the day (1000–1700 hours), the value is always positive. The magnitude of VOC chemistry values represents how much VOCs has been removed through local chemical and photochemical processes. The value is always negative, meaning that VOCs are consumed.

[39] Figures 12 and 13 present mean daily total O_3 production by chemistry (P_{O_3}) and mean VOC loss (L_{VOC}) due to chemistry during the photochemically active period of the day (1000–1700 hours) over the entire modeling period for each scenario, respectively. Each location has its own characteristics in terms of the intensity and variation trend with different scenarios. Of the three locations, MACA consistently has the largest P_{O_3}, GRSM the least, with SHEN in between. However, the largest L_{VOC} always appears at SHEN. For most of the scenarios, the L_{VOC} values are smallest at GRSM and in between at MACA. As discussed earlier, reactive VOCs react not only with OH to produce O_3 but the intermediate products of VOCs react also with NO_x as well. The explanation of higher VOC chemistry but lower O_3 production due to chemistry at SHEN lies in the fact that reactive VOC species are a larger share of total VOCs and NO_x concentrations are lower at this location than at MACA. Referring back to Figure 5, we find that isoprene concentrations at SHEN (mean midday concentration: 3.36 ppbv) are indeed much higher than those at MACA (mean midday concentration: 0.78 ppbv).

[40] The relationship between net O_3 production (P_{O_3}) and VOC loss (L_{VOC}) due to chemistry at the three locations is presented in Figure 14. The last scenario, CS8, is not included because this scenario significantly reduces O_3 production at all three locations. Note that VOCs are consumed in VOC chemistry, but O_3 is produced in O_3 chemistry (for convenience sake, the negative sign of the VOC chemistry term is dropped). It is clear that the consumption of VOCs contributes to an approximately linear increase in O_3 production at all three locations, but their actual relationship varies from location to location.

[41] We define a new term called VOC potential for O_3 production (VPOP) as

$$\mathrm{VPOP} = \frac{dP_{O_3}}{dL_{VOC}}. \tag{4}$$

VPOP is a measure of the change in O_3 production per unit change of VOCs consumed or, in other words, the O_3

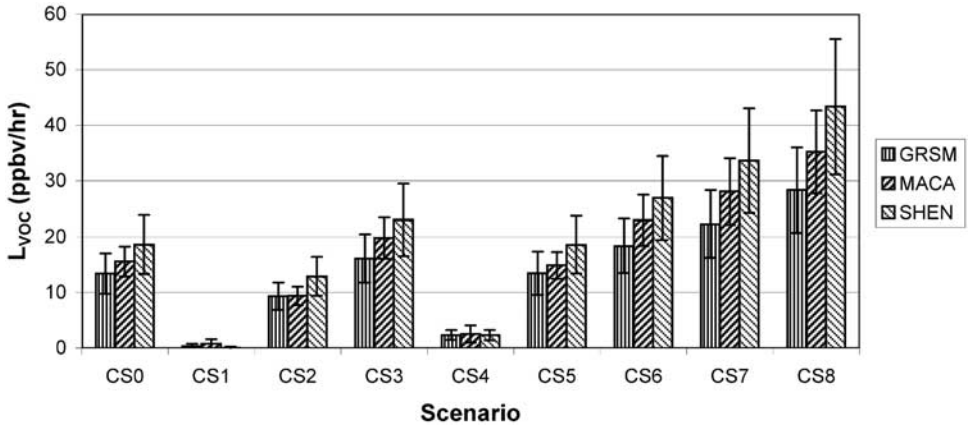

Figure 13. Model-predicted mean daytime VOC chemistry (L_{VOC}). Model output from 1000 to 1700 hours of each day is used to calculate the mean, and the negative sign is dropped. Error bars are the standard deviations.

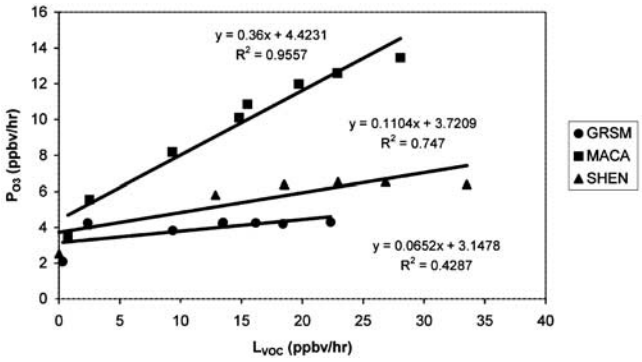

Figure 14. O_3 chemistry and VOC chemistry (the negative sign for L_{VOC} is dropped).

production efficiency of VOC chemistry. It represents the slope of the best fitted regression line through the data in Figure 14.

[42] From Figure 14, the VPOP values are 0.065 (GRSM), 0.36 (MACA), and 0.11 (SHEN) ppbv O_3 per ppbv VOCs. Thus one ppbv VOCs consumed produces 5.5 times more O_3 at MACA than at GRSM. It is interesting to note that if VOC chemistry is zero, values for O_3 production due to chemistry are similar at all three locations (3.1–4.4 ppbv/h). These may represent background O_3 production from inorganic reactions such as CO and CH_4 [*Goldan et al.*, 2000].

[43] VPOP values for the entire modeling domain are presented in Figure 15. Larger VPOP values are found in the northwest region of this domain as well as in the southeast region over the ocean corresponding to lower VOC emissions. Figure 15 gives the relative importance of VOCs in O_3 production, and this implies what the effective ways are to control O_3. In regions with higher VPOP values, it may be more effective to control O_3 by reducing VOC emissions; on the other hand, lower VPOP values generally mean that local O_3 production is low due to reactions of VOCs, and hence it may not be effective to control O_3 by reducing VOCs.

5. Conclusions and Implications

[44] The air-quality model MAQSIP is shown to predict O_3 concentrations with an overall uncertainty of less than 30% and daily average O_3 concentrations with even less uncertainty. The diurnal variation patterns at both low- and high-elevation locations are simulated reasonably well by the modeling system. Limited comparisons between predicted and measured VOCs indicate that the predictions of VOC species concentrations are less successful. Out of six nonmethane hydrocarbon species, PAR is best predicted within a factor of 2 in most cases, followed by isoprene being underestimated by a factor of 3–5. Most other species are predicted at about one order of magnitude lower than observed values. However, the fractional reactivity of the various VOC species is captured properly by MAQSIP. The comparison of the observed and model-predicted RWOG suggests that the model Base Scenario underestimates RWOG by a factor of 3–10 for the three locations studied.

[45] Model predictions show a MVCP, that is, the point at which further addition of VOCs reduces O_3 concentration at all locations. Among the three locations, model calculation suggests that the largest O_3 production due to local chemistry processes occurs at MACA and is almost double that at GRSM or SHEN. Even with the Base Scenario, which underestimates the emissions of most of the reactive VOC species, the MVCP appears to have been reached at GRSM. If we consider CS8 to be scenario closest to observed values at each location, then VOCs are all chemically saturated in terms of O_3 production at all locations and can lead to reduced O_3 production with further increase in emissions.

[46] The intensity of the VOC chemistry process, which ranks SHEN first, MACA second, and GRSM last, is a measure of how actively VOCs participate in local chemical reactions. The VPOP, which is three and six times greater at MACA than at SHEN and GRSM, respectively, measures the efficiency of O_3 production due to the chemistry process of VOCs. These two metrics can be used to quantitatively evaluate the relative strength of chemistry process and O_3 production at a location. The map of VPOP for the entire modeling domain present a clear picture of relative O_3 productivity and intensity of chemistry processes. Within the context of the entire modeling domain, all three national park locations are at the lower side of all these metrics.

[47] Model sensitivity and budget analyses indicate that more than half of the local O_3 is transported from other areas for the two high-elevation sites (GRSM and SHEN) and just 20% for the low-elevation site (MACA); local chemistry or photochemical reactions contribute 26–43% of the local O_3 at GRSM and SHEN and 81% at MACA. Vertical transport and dry deposition are responsible for removal of O_3 from atmosphere. Local emissions contribute 67–95% of VOCs, with the remainder attributed to advection and diffusion processes. About 50% of the VOCs are consumed by local chemistry processes, 30–50% by horizontal or vertical transport, and less than 10% by dry deposition. The relative capacity of local O_3 production is closely related to the characteristics of VOCs at each location. For instance, compared with GRSM and SHEN, higher local O_3 production at MACA is also signified by its higher values of VPOP and MVCP, and the values of these metrics at a location are in turn dependent on NO_x levels of this location.

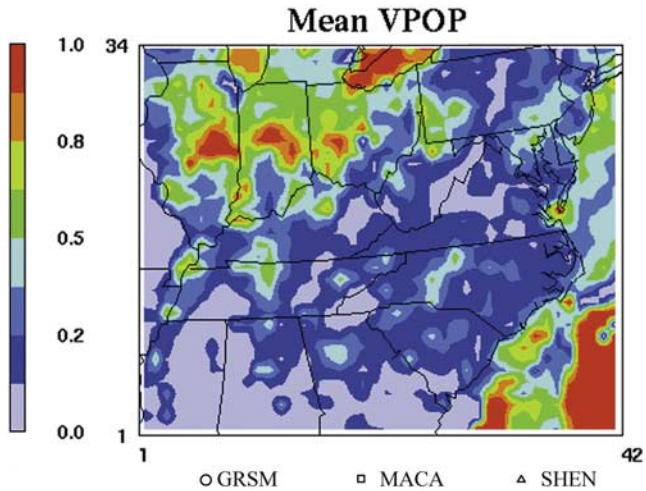

Figure 15. Mean VPOP values over the entire modeling domain.

[48] This study has several important implications. There are distinctive characteristics of O_3 distribution, transport, and production for locations with different elevation. In areas where transport dominates local O_3 production, the most effective strategy is to reduce O_3 levels in the source areas from which it is transported. However, in areas that O_3 is predominantly produced locally, reducing NO_x or VOC levels according to their characteristics in the location may help reduce values of VPOP and MVCP, and thus reduce the capacity of O_3 production. The existence of MVCP points, which is contrary to previous understanding of the atmospheric chemistry of O_3 production, implies that large amounts of reactive biogenic VOCs that often exist in densely vegetated environments during summer, may help regulate O_3 levels under NO_x-limited conditions.

[49] Further research is needed to improve the emissions inventory, reduce large uncertainty in biogenic emissions, and more fully account for locally emitted VOCs. Further model sensitivity analysis is also needed to take into consideration the effect of NO_x, CO, and other species.

[50] **Acknowledgments.** This research was funded by the National Park Service, Air Resources Division cooperative agreement 4000-7-9003 and by the Canon National Parks Science Scholars Program, National Park Foundation contract 92899. Many people contributed to the fieldwork of this study, including Bob Carson, Jim Renfro, Shane Spitzer, and Scott Berenyi (station operators); Rod Zika and Charlie Farmer (VOC analysis); and Ken Olszyna, for partnership operation of the sites. Thanks to M. Defeo for the word processing of the manuscript. Mention of trade names of commercial products does not constitute endorsement or recommendation for use.

References

Altshuller, A. P., The role of nitrogen oxides in nonurban ozone formation in the planetary boundary layer over N America, W Europe and adjacent areas of ocean, *Atmos. Environ.*, *20*, 245–268, 1986.

Aneja, V. P., R. G. Oommen, A. J. Riordan, S. P. Arya, R. J. Wayland, and G. C. Murray, Ozone patterns for three metropolitan statistical areas in North Carolina, USA, *Atmos. Environ.*, *33*, 5081–5093, 1999.

Aneja, V. P., S. P. Arya, Y. Li, G. C. Murray, and T. L. Manuszak, Climatology of diurnal trends and vertical distribution of ozone in the atmosphere boundary layer in urban North Carolina, *J. Air Waste Manage. Assoc.*, *50*, 54–64, 2000a.

Aneja, V. P., R. Mathur, S. P. Arya, Y. Li, G. C. Murray, and T. L. Manuszak, Coupling the vertical distribution of ozone in the atmospheric boundary layer, *Environ. Sci. Technol.*, *34*, 2324–2329, 2000b.

Aneja, V. P., A. A. Adams, and S. P. Arya, An observational based analysis of ozone trends and production for urban areas in North Carolina, *Chemosphere*, *2*, 157–165, 2000c.

Apel, E. C., J. G. Calvert, R. Zika, M. O. Rodgers, V. P. Aneja, J. F. Meagher, and W. A. Lonneman, Hydrocarbon measurements during the 1992 Southern Oxidants Study Atlanta Intensive: Protocol and quality assurance, *J. Air Waste Manage. Assoc.*, *45*, 521–528, 1995.

Arya, S. P., *Air Pollution Meteorology and Dispersion*, Oxford Univ. Press, New York, 1999.

Byun, D. W., and J. K. S. Ching (Eds.), Science algorithms of the EPA Models-3 Community Multi-scale Air Quality (CMAQ) modeling system, *Rep. EPA/600/R-99/030*, Off. of Res. and Dev., U.S. Environ. Prot. Agency, Research Triangle Park, N. C., 1999.

Chameides, W. L., R. W. Lindsay, J. Richardson, and C. S. Kiang, The role of biogenic hydrocarbons in urban photochemical smog: Atlanta as a case study, *Science*, *241*, 1473–1474, 1988.

Chameides, W. L., R. D. Saylor, and E. B. Cowling, Ozone pollution in the rural united states and the new NAAQS, *Science*, *276*, 916, 1997.

Chang, J. S., R. A. Brost, I. S. A. Isaksne, S. Madronich, P. Middleton, W. R. Stockwell, and C. J. Walcek, A three-dimensional Eulerian Acid Deposition Model: Physical concepts and formulation, *J. Geophys. Res.*, *92*, 14,681–14,700, 1987.

Cowling, E. B., W. L. Chameides, C. S. Kiang, F. C. Fehsenfeld, and J. F. Meagher, Introduction to special section: Southern Oxidants Study Nashville/Middle Tennessee Ozone Study, *J. Geophys. Res.*, *103*, 22,209–22,212, 1998.

Dennis, R. L., D. W. Byun, J. H. Novak, K. J. Galluppi, C. J. Coats, and M. A. Vouk, The next generation of integrated air quality modeling: EPA's Models-3, *Atmos. Environ.*, *30*, 1925–1938, 1996.

Dimitriades, B., Photochemical oxidant formation: Overview of current knowledge and emerging issues, in *Atmospheric Ozone Research and Its Policy Implications*, edited by T. Schneider et al., Elsevier Sci., New York, 1989.

Dodge, M. C., Combined use of modeling techniques and smog chamber data to derive ozone precursor relationships, in *Proceedings of the International Conference on Photochemical Oxidant Pollution and Its Control*, edited by B. Dimitriades, vol. 2, *Rep. EPA-600/3-77-0016*, pp. 881–889, U.S. Environ. Prot. Agency, Research Triangle Park, N. C., 1977.

Farmer, C. T., P. J. Milne, D. D. Riemer, and R. G. Zika, Continuous hourly analysis of C2–C10 nonmethane hydrocarbon compounds in urban air by GC-FID, *Environ. Sci. Technol.*, *28*, 234–245, 1994.

Fehsenfeld, R. M., J. Calvert, R. Fall, P. Goldan, A. Guenther, B. Lamb, S. Liu, M. Trainer, H. Westberg, and P. Zimmerman, Emissions of volatile organic compounds from vegetation and the implications for atmospheric chemistry, *Global Biogeochem. Cycles*, *6*, 389–430, 1992.

Fuentes, J. D., et al., Biogenic hydrocarbons in the atmospheric boundary layer: A review, *Bull. Am. Meteorol. Soc.*, *81*, 1537–1575, 2000.

Geron, C. D., A. B. Guenther, and T. E. Pierce, An improved model for estimating emissions of volatile organic compounds from forests in the eastern United States, *J. Geophys. Res.*, *99*, 12,773–12,791, 1994.

Gery, M. W., G. Z. Whitten, J. P. Killus, and M. C. Dodge, A photochemical kinetics mechanism for urban and regional scale computer modeling, *J. Geophys. Res.*, *94*, 12,925–12,956, 1989.

Goldan, P. D., D. D. Parrish, W. C. Kuster, M. Trainer, S. A. McKeen, J. Holloway, B. T. Jobson, D. T. Sueper, and F. C. Fehsenfeld, Airborne measurements of isoprene, CO, and anthropogenic hydrocarbons and their implications, *J. Geophys. Res.*, *105*, 9091–9105, 2000.

Guenther, A., C. Geron, T. Pierce, B. Lamb, R. Harley, and R. Fall, Natural emissions of non-methane volatile organic compounds, carbon monoxide, and oxides of nitrogen from North America, *Atmos. Environ.*, *34*, 2205–2230, 2000.

Hagerman, L. M., V. P. Aneja, and W. A. Lonneman, Characterization of non-methane hydrocarbons in the rural southeast United States, *Atmos. Environ.*, *31*, 4017–4038, 1997.

Heck, W. W., W. W. Cure, J. O. Rawlings, L. J. Zaragoza, A. S. Heagle, H. E. Heggestad, R. J. Kohut, and P. J. Temple, Assessing impacts of ozone on agriculture crops, II, crop yield functions and alternative exposure statistics, *J. Air Pollut. Control Assoc.*, *34*, 810–817, 1984.

Henry, R. C., C. H. Spiegelman, J. F. Collins, and E. Park, Reported emissions of organic gases are not consistent with observations, *Proc. Natl. Acad. Sci. U. S. A.*, *94*, 6596–6599, 1997.

Hogrefe, C., S. T. Rao, P. Kasibhatla, G. Kallos, G. J. Tremback, W. Hao, D. Olerud, A. Xiu, J. McHenry, and K. Alapaty, Evaluating the performance of regional-scale photochemical modeling systems, part I, Meteorological predictions, *Atmos. Environ.*, *35*, 4159–4174, 2001a.

Hogrefe, C., S. T. Rao, P. Kasibhatla, W. Hao, G. Sistla, R. Mathur, and J. McHenry, Evaluating the performance of regional-scale photochemical modeling systems, part II, Ozone predictions, *Atmos. Environ.*, *35*, 4175–4188, 2001b.

Houyoux, M. R., C. J. Coats, A. Eyth, and S. C. Y. Lo, Emissions modeling for SMRAQ: A seasonal and regional example using SMOKE, paper presented at AMWA Computing in Environmental Resources and Management Conference, Research Triangle Park, N. C., 2–4 Dec., 1996.

Houyoux, M. R., J. M. Vukovich, C. J. Coats Jr., N. J. M. Wheeler, and P. S. Kasibhatla, Emission inventory development and processing for the Seasonal Model for Regional Air Quality (SMRAQ) project, *J. Geophys. Res.*, *105*, 9079–9090, 2000.

Kang, D., V. P. Aneja, R. G. Zika, C. Farmer, and J. D. Ray, Nonmethane hydrocarbons in the rural southeast United States national parks, *J. Geophys. Res.*, *106*, 3133–3155, 2001.

Kasibhatla, P., and W. L. Chameides, Seasonal modeling of regional ozone pollution in the eastern United States, *Geophys. Res. Lett.*, *27*, 1415–1418, 2000.

Kasibhatla, P., W. L. Chameides, B. Duncan, M. Houyoux, C. Jang, R. Mathur, T. Odman, and A. Xiu, Impact of inert organic nitrate formation on ground-level ozone in a regional air quality model using the carbon bond mechanism 4, *Geophys. Res. Lett.*, *24*, 3205–3208, 1997.

Lamb, B., D. Gay, H. Westberg, and T. Pierce, A biogenic hydrocarbon emission inventory for the USA using a simple forest canopy model, *Atmos. Environ.*, *27*, 1709–1713, 1993.

Lamb, R. G., Numerical simulations of photochemical air pollution in the northeastern United States: ROM1 applications, *Rep. EPA-600/3-86-038*, U.S. Environ. Prot. Agency, Research Triangle Park, N. C., 1986.

Lin, X., M. Trainer, and S. C. Liu, On the nonlinearity of the tropospheric ozone production, *J. Geophys. Res.*, *93*, 15,879–15,888, 1988.

Liu, S. C., M. Trainer, F. C. Fehsenfeld, D. D. Parrish, E. J. Williams, D. W. Fahey, G. Huber, and P. C. Murphy, Ozone production in the rural troposphere and implications for regional and global ozone distributions, *J. Geophys. Res.*, *92*, 4194–4207, 1987.

Mathur, R., K. L. Schere, and A. Nathan, Dependencies and sensitivity of tropospheric oxidants precursor concentrations over the northeast United States: A model study, *J. Geophys. Res.*, *99*, 10,535–10,552, 1994.

McKeen, S. A., G. Wotawa, D. D. Parrish, J. S. Holloway, M. P. Buhr, G. Hubler, F. C. Fehsenfeld, and J. F. Meagher, Ozone production from Canadian wildfires during June and July of 1995, *J. Geophys. Res.*, *107*(D14), doi:10.1029/2001JD000697, 2002.

Meagher, J. F., E. B. Cowling, F. C. Fehsenfeld, and W. J. Parkhurst, Ozone formation and transport in southeastern United States: Overview of the SOS Nashville/Middle Tennessee Ozone Study, *J. Geophys. Res.*, *103*, 22,213–22,223, 1998.

Morris, R. E., and T. C. Myers, User's guide for the Urban Airshed Model, vol. 1, User's manual for UAM (CBM-IV), *Rep. EPA 450/4-90/007A*, U.S. Environ. Prot. Agency, Research Triangle Park, N. C., 1992. (Available as *PB91-131227/REB* from Natl. Tech. Inf. Serv., Springfield, Va.)

National Research Council, *Rethinking the Ozone Problem in Urban and Regional Air Pollution*, Natl. Acad. Press, Washington, D. C., 1991.

Odman, T., and C. L. Ingram, Multiscale air quality simulation platform (MAQSIP): Source code documentation and validation, *MCNC Tech. Rep., ENV-96TR002-v1.0*, 1996.

Russell, A., and R. Dennis, NARSTO critical review of photochemical models and modeling, *Atmos. Environ.*, *34*, 2283–2324, 2000.

St. John, J. C., W. L. Chameides, and R. Saylor, Role of anthropogenic NO_x and VOC as ozone precursors: A case study of the SOS Nashville/Middle Tennessee ozone study, *J. Geophys. Res.*, *103*, 22,415–22,423, 1998.

Tesche, T. W., D. E. McNally, and R. A. Emigh, Assessment of the OTAG modeling Paper 9A4, in *Proceedings of 10th Conference on Application of Air Pollution Meteorology*, vol. 45, pp. 480–489, Am. Meteorol. Soc., Boston, Mass., 1998.

Tonnesen, S., and R. L. Dennis, Analysis of radical propagation efficiency to assess ozone sensitivity to hydrocarbons and NO_x: 1. Local indicators of instantaneous odd oxygen production sensitivity, *J. Geophys. Res.*, *105*, 9213–9225, 2000a.

Tonnesen, S., and R. L. Dennis, Analysis of radical propagation efficiency to assess ozone sensitivity to hydrocarbons and NO_x: 2. Long-lived species as indicators of ozone concentration sensitivity, *J. Geophys. Res.*, *105*, 9227–9241, 2000b.

Tonnesen, S., and E. H. Jefferies, Inhibition of odd oxygen production in the carbon four and generic reaction set mechanisms, *Atmos. Environ.*, *28*, 1339–1349, 1994.

Trainer, M., E. J. Williams, D. D. Parrish, M. P. Buhr, E. J. Allwine, H. H. Westberg, F. C. Fehsenfeld, and S. C. Liu, Models and observations of the impact of natural hydrocarbons on rural ozone, *Nature*, *329*, 705–707, 1987.

Trainer, M., D. D. Parrish, P. D. Goldan, J. Roberts, and F. C. Fehsenfeld, Review of observation-based analysis of the regional factors influencing ozone concentrations, *Atmos. Environ.*, *34*, 2045–2061, 2000.

United States Environmental Protection Agency (U.S. EPA), Guidance on Urban Airshed Model (UAM) reporting requirements for attainment demonstrations, *Rep. EPA-450/4-91-013*, U.S. Environ. Prot. Agency, Research Triangle Park, N. C., July 1991.

Venkatram, A., P. K. Karamchandani, and P. K. Misra, Testing a comprehensive acid deposition model, *Atmos.*, 22,737–22,747, 1988.

Whitten, G. Z., H. P. Deuel, C. S. Burton, and J. L. Haney, Overview of the implementation of an updated isoprene chemistry mechanism in CB4/UAM-V, report, Syst. Appl. Intl. (SAI), San Rafael, Calif., 1996.

V. P. Aneja, Department of Marine, Earth, and Atmospheric Sciences, North Carolina State University, Raleigh, NC 27695-8208, USA. (viney_aneja@ncsu.edu)

D. Kang, Atmospheric Modeling Division, U.S. EPA, Mail Drop E243-01, Research Triangle Park, NC 27711, USA.

R. Mathur, Carolina Environmental Program, University of North Carolina, Chapel Hill, NC 27599-1105, USA.

J. D. Ray, Air Resources Division, National Park Service, Denver, CO 80225-0287, USA.